Research Square

Preprints are preliminary reports that have not undergone peer review.
They should not be considered conclusive, used to inform clinical practice,
or referenced by the media as validated information.

Studies in biological interactions of apigenin by spectroscopic, quantum chemical calculations and molecular docking

Priya Verma
University of Lucknow
Preeti Prajapati
University of Lucknow
Anubha Srivastava
University of Lucknow
Jaishree Jadham
Vikram University
Meenu Purohit
Vikram University
Uma Sharma
umasharma10@rediffmail.com

Vikram University

Research Article

Keywords: Apigenin, IR spectroscopy, UV-Visible spectra, chemical reactivity, molecular docking

Posted Date: November 18th, 2026

DOI: https://doi.org/10.21203/rs.3.rs-11612920/v1

License: This work is licensed under a Creative Commons Attribution 4.0 International License.
Read Full License

Additional Declarations: No competing interests reported.

Studies in biological interactions of apigenin by spectroscopic, quantum chemical calculations and molecular docking

Priya Verma[1], Preeti Prajapati[2], Anubha Srivastava[2], Jaishree Jadham[1], Meenu Purohit[1], Uma Sharma[1*]
[1*]School of studies in Chemistry and Biochemistry, Samrat Vikramaditya University, Ujjain, 456010, India.
[2]Department of Physics, University of Lucknow, Lucknow, 226007, India.

*** Correspondence:**
Uma Sharma: umasharma10@rediffmail.com
Priya Verma: priyaverma220192@gmail.com

Abstract

Apigenin (APG) is a naturally plant dietary flavonoid widely distributed in various plants and foods, including celery, parsley and chamomile. This study investigates the structural, spectroscopic, electronic and reactivity properties of the monomeric and dimeric APG using experimental and DFT methods at the B3LYP/6-311G(d,p) level. The APG dimer was stabilized by intermolecular hydrogen bonding through (O-H···O) and (C-H···O) interactions. Quantum theory of atoms in molecules (QTAIM) analysis revealed significant intermolecular hydrogen bonding interaction (O3-H4···O5) in the dimer. Natural bond orbital analysis further indicated that intermolecular hydrogen bonding contributes significantly to the stabilization of the APG dimer. Vibrational and UV-Vis spectroscopy were also analyzed to assess the structural and electronic characteristics of monomer and dimer models of APG. HOMO-LUMO analysis of the APG monomer and dimer was performed to evaluate their electronic structure, reactivity and stability. The electrophilic and nucleophilic reactivity and site selectivity of molecule were revealed by molecular electrostatic potential (MESP) map. To get insights into biological properties, molecular docking of APG was performed. Overall, the results demonstrate that intermolecular hydrogen bonding plays an important role in the structural stabilization and electronic properties of the APG dimer and provides useful insights into the molecular interactions and reactivity of APG.

Keywords: Apigenin, IR spectroscopy, UV-Visible spectra, chemical reactivity, molecular docking

1. Introduction

Natural product are bioactive compounds obtained from natural sources such as plants, fungi, microorganisms and animals [1,2]. Their diverse chemical structures and biological activities make them important in pharmaceutical research, cosmetics and functional foods, particularly for for drug discovery [3]. Apigenin (APG, 4',5,7-trihydroxyflavone) is a naturally occurring flavonoid widely distributed in plants such as celery, parsley and chamomile. APG is a yellow crystalline compound with reported antioxidant, anti-inflammatory, antidiabetic and anticancer activities [4-6]. Its biological effects have attracted considerable interest in pharmacological and drug-discovery research. However, its limited aqueous solubility may restrict its bioavailability and therapeutic applications. Therefore, understanding the structural, spectroscopic and electronic properties of APG is important for elucidating its molecular behavior and potential applications [7-9]. The chemical structure of APG is shown in Fig. 1.

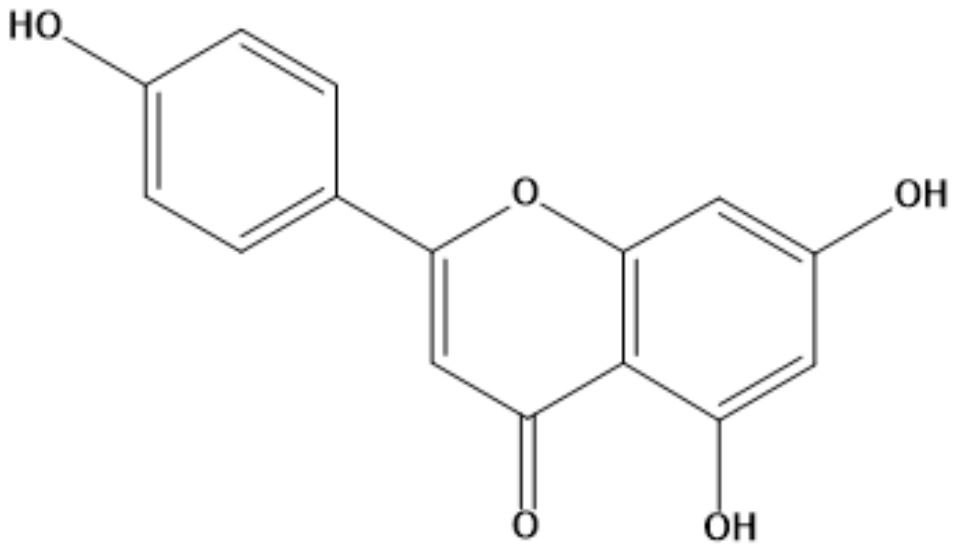


Fig. 1. The chemical structure of apigenin.

In the solid state APG crystallizes to monoclinic crystal system with space group Cc and unit cell parameters a = 3.7258 Å, b = 70.43 Å, c = 17.546 Å and α = 90˚, β = 94.028 Å, γ = 90˚ [10]. Its

crystal structure is shown in Fig. S1. APG has been studied by various researchers; Salehi et al. proposed the therapeutic potential of APG, and highlighted the key role in dietary health assessment [8]. Jiang et al. have studied the potential evaluation of APG as a model medicine for atherosclerosis [11]. Lin et al. have reported insights into pharmaceutical properties of APG in context of osteoporosis [12].

The molecular geometry and wavenumber analysis has been done by DFT/B3LYP/6-311++G(d,p) methodology by using FT-IR and FT-Raman approach [13]. The vibrational (FT-IR and FT-Raman) spectra of model drug (APG) are a unique fingerprinting of molecular vibrations, which uniquely determines the molecules geometry and functional groups. Density functional theory (DFT) method is defined as the computational approach, used to study the ground state properties of molecules with the use of electron density [14].

Natural products have been a topic of great study for researchers and several natural products like paclitaxel (from the Pacific yew), morphine (form the Opium poppy) artemisinin (Artemisia annua) and quinine (from Cinchona tree) have been studied [15,16]. The present work is focused to study molecular structure, their geometries, spectroscopic signatures and chemical reactivity by using experimental and quantum chemical approach. The natural bond orbital (NBO) analysis has been done to achieve the stabilization energy $E^{(2)}$ and the strength of hydrogen bonds [17]. The frontier molecular orbital analysis has been done by highest occupied molecular orbital (HOMO) and lowest unoccupied molecular orbital (LUMO) showed the chemical reactivity, charge transfer and stability of the molecule [18]. The chemical reactivity descriptors (global and local) plays pivotal role to define overall electronic behavior and chemical reactivity of molecular system [19]. Furthermore, the local reactivity descriptors reveal the atomic sites prone to nucleophilic, electrophilic and radical attacks [20]. Molecular docking refers to computational technique that identifies how two molecules, like ligand (drug) and a receptor (protein) binds to form stable structure [21,22]. The docking analysis of APG was performed with with death-associated protein Kinase-1 (PDB code: 5AUT) [23], severe acute respiratory syndrome coronavirus 2 (SARS-CoV-2, PDB code: 7ZH5) [24] and acetylcholinesterase (PDB code: 1EEA) [25] to observed the action-mechanism of aforesaid molecule. These results provide that the insights into experimental and theoretical approach to study APG molecule, with future scope

of studying novel drug molecules, hence exploring the molecular system in chemical, biological and pharmaceutical field.

2. Experimental techniques

2.1 Material used

Apigenin (purity 99%) was purchased from Alfa-acer and used without further purification. Solid-state grinding experiment was carried out using a mortar and pestle. The 2.5 mg of APG were added to the mortar and thoroughly ground together with the pestle until a homogeneous mixture was obtained.

2.2 Fourier-transform infrared (FT-IR) spectroscopy

The FT-IR spectrum of the APG was obtained using a Bruker Vertex 80v Fourier-transform infrared spectrometer fitted with a deuterated lanthanum α-alanine-doped triglycine sulfate (DLaTGS) detector and a platinum attenuated total reflectance (Pt-ATR) accessory. Spectral measurements were performed over the wavenumber range of 400–4000 cm^{-1} at an optical resolution of 4 cm^{-1}. All spectra were collected under vacuum using a double-sided forward–backward scanning mode.

2.3 UV-Vis spectroscopy

UV-Visible spectra were recorded using a double beam JASCO V-760 spectrophotometer over the wavelength range of 190-400 nm at room temperature. Measurements were performed using a quartz cuvette with a 1 cm optical path length. Baseline correction was performed using the corresponding buffer solution as the reference in the second beam. All measurements were conducted under identical instrumental conditions with a slit width of 1 nm.

3 Computational and theoretical details

The ground state optimized structure of monomer and dimer of APG were obtained using DFT and Becke's three parameters Lee-Yang-Parr (B3LYP) with the 6-311G(d,p) basis set [26-28]. All calculations were performed using the Gaussian 09 program [29]. The optimized molecular structures were visualized using GaussView [30].

The spectroscopic fingerprints (Infrared spectra) and potential energy distribution (PED) were obtained using the Gar2Ped program following Pulay's recommendations [31]. The differences between the experimentally observed and computed theoretically calculated wavenumbers arise mainly from the use of an isolated molecule in the gas phase for the theoretical calculations, whereas the experimental measurements were performed for the molecule in the solid state. In addition, anharmonic effects and the approximations associated with the computational method contribute to these discrepancies. Therefore, a linear scaling procedure (WLS) [32] was employed to scale the calculated vibrational wavenumbers and improve their agreement with the experimental values.

The electron density, topological properties and characteristics by hydrogen bonding were analyzed by using the AIM2000 program [33]. The nature and strength of the hydrogen bonds were further evaluated through the electron density at the bond critical point (BCP). According to Espinosa et al., the hydrogen bond energy (E_{HB}) is related to the potential energy density (V_{BCP}) at H···O contact by the following relationship [34].

$$E_{HB} = 0.5\ V_{BCP}$$

The global parameters, including electronegativity (χ), chemical potential (μ), hardness (η), electrophilicity index (ω) and softness (S) were evaluated from the energies the highest occupied molecular orbital (HOMO) and lowest unoccupied molecular orbital (LUMO) using the following equations [35,36]:

$$\boldsymbol{\chi = -\frac{1}{2}(E_{HOMO} + E_{LUMO})} \qquad \textbf{(i)}$$

$$\boldsymbol{\mu = -\chi = \frac{1}{2}(E_{HOMO} + E_{LUMO})} \qquad \textbf{(ii)}$$

$$\boldsymbol{\eta = \frac{1}{2}(E_{LUMO} - E_{HOMO})} \qquad \textbf{(iii)}$$

$$\boldsymbol{S = \frac{1}{2\eta}} \qquad \textbf{(iv)}$$

$$\boldsymbol{\omega = \frac{\mu^2}{2\eta}} \qquad \textbf{(v)}$$

The electrophilicity index (ω) is a global reactivity descriptor that quantifies the stabilization energy associated with the maximum electron transfer from the surrounding environment to an electrophilic system. The maximum amount of electronic charge (ΔN_{max}) that can be accepted by an electrophile is expresses as:

$$\Delta N_{max} = -\frac{\mu}{\eta} \qquad \textbf{(vi)}$$

where, μ and η represent the chemical potential and global hardness, respectively.

The NBO analysis was performed at the same level of theory to elucidate the electronic structure and donor-acceptor interactions. Molar refractivity (MR) is an important molecular descriptor that provides information about molecular polarizability and steric properties and is frequently employed in quantitative structure-activity relationship (QSAR) studies. It can be calculated using Lorentz-Lorenz equation as follows [37]:

$$MR = \left[\frac{n^2-1}{n^2+2}\right]\left(\frac{MW}{\rho}\right) = 1.333\pi N\alpha \qquad \textbf{(vii)}$$

where n is the refractive index, MW is the molecular weight, ρ is the density, N is Avogadro's number and α is the molecular polarizability.

To investigate the potential biological activity of the title molecule, molecular docking studies were performed using AutoDock4.2 software [38]. The corresponding active-site residues and ligand-protein interactions were subsequently analyzed and visualized using Discovery Studio Visualizer 4.5 software [39].

4. Results and discussion

4.1 Geometry optimization and energies

The crystal structure of APG was previously investigated by Makadia et al. [10] and reported to crystallize in the monoclinic crystal system with Cc space group. The unit cell parameters were determined as a = 3.7258(12) Å, b = 70.43(2) Å, c = 17.546(5) Å, with cell angles α = 90˚, β = 94.028˚(13), γ = 90˚. The crystal packing is stabilized by intermolecular hydrogen bonding

interactions between the carbonyl (C=O) and hydroxyl (OH) groups of neighboring APG molecules, as illustrated in Fig. S1.

The optimized geometrical parameters, including bond-lengths, bond-angles and dihedral-angles obtained at the DFT/B3LYP/6-311G(d,p) level of theory for both the monomeric and dimeric models of APG are summarized in Table S1. The optimized molecular structures of the APG monomer and dimer are presented in Figs. 1 and 2, respectively. The calculated molecular energies of the monomer and dimer were found to be -598498.2341 and -1197010.4131 kcal/mol, respectively.

The binding energy (B.E.) of the APG dimer was calculated from the difference between the total energy of the dimer and the sum of the energies of the two isolated monomers. The calculated B.E. was found to be -13.9449 kcal mol^{-1}, indicating favorable intermolecular interactions and stabilization of the dimeric structure. Since, the basis set superposition error (BSSE) play a pivotal role in energy [40], hence the counterpoise correction was carried out and B.E. found to be -10.4785 kcal mol^{-1} with BSSE correction of 3.4634 kcal mol^{-1}. These results confirm that the intermolecular interactions contribute significantly to the stability of the APG dimer.

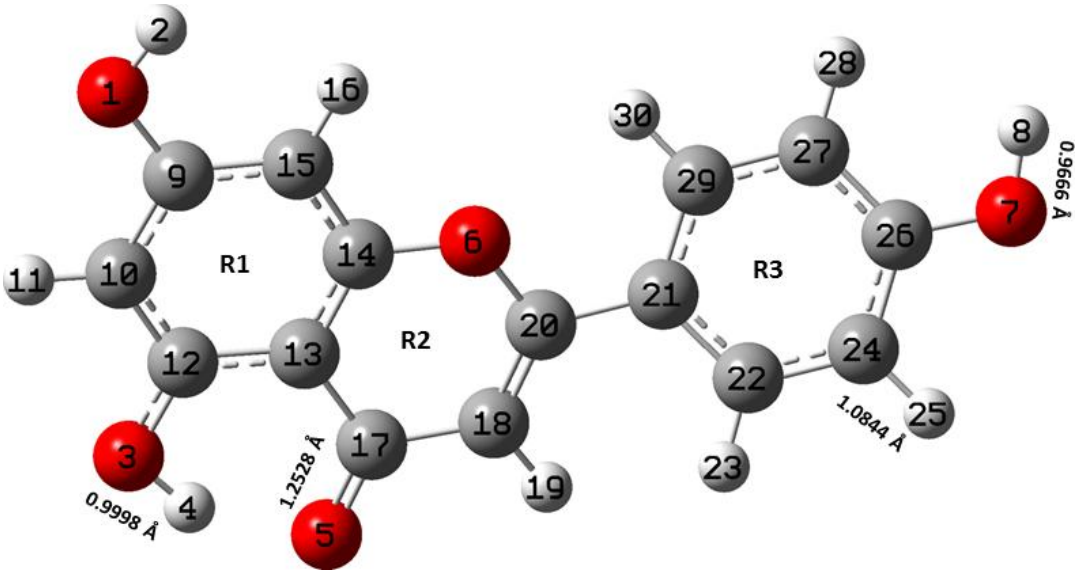


Fig. 2. Optimized structure for monomer model of APG with the atomic numbering scheme adopted in the present study.

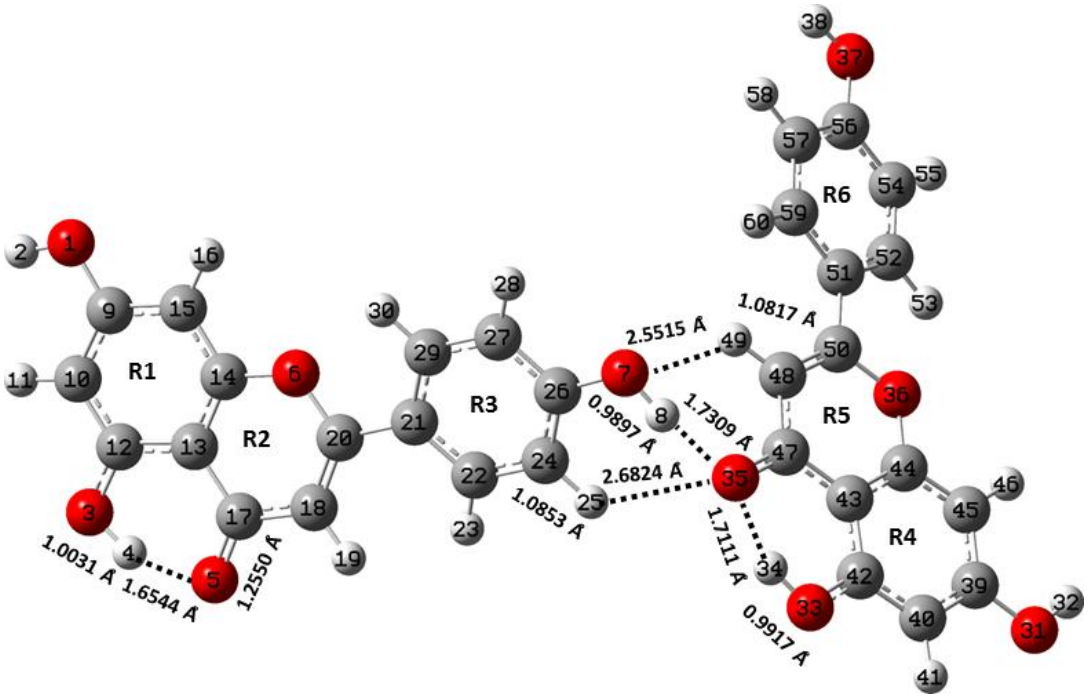


Fig. 3. Optimized structure for dimer model of APG with the atomic numbering scheme adopted in the present study.

The structural parameters, including bond-lengths, bond-angles and dihedral-angles, obtained from the optimized monomeric and dimeric models he results demonstrate a good overall agreement between the calculated and experimental geometries, with deviations of 0.3699/0.0133 Å in bond-length, 6.88/1.38˚ in bond-angles and 14.78/12.91˚ in dihedral-angles, respectively (as shown in Table S1).

In monomer/dimer of APG, the major deviations in experimental and calculated bond-length values were noticed among bonds; (O3-H4)/(O3-H4, O33-H34), (O5=C17)/(O5=C17, O35=C47), (O7-H8)/(O7-H8, O37-H38) and (C24-H25)/(C24-H25, C57-H58) by (0.1604/0.5219, 0.1523), (0.3890/0.0269, 0.0128), (0.5267/0.1511, 0.1282) and (0.4361/0.1354, 0.1345), respectively. These variations can primarily be attributed to difference between the isolated molecular environment considered in the theoretical calculations and the intermolecular interactions present in the crystalline state. The corresponding variations were also observed in the associated bond-angles and dihedral-angles.

The deviations in the geometrical parameters were considerably reduced in the dimeric model of APG (shown in Fig. 3), highlighting the important role of intermolecular hydrogen bonding

interactions in reproducing the experimental crystal geometry. In particular, hydrogen bonds involving (O3-H4···O5), (O33-H34···O35), (O7-H8···O35), (C48-H49···O7) and (C24-H25···O35) contributed to the stabilization of the dimeric structure. In contrast, the monomeric model (Fig. 2), which does not account for these intermolecular interactions, exhibited comparatively larger deviations from the experimental crystal structure.

4.2 Vibrational assignments and wavenumbers

APG monomer and dimer molecules contain 30 and 60 atoms, hence it give 84 and 174 (3N-6), normal modes, respectively. Detailed vibrational assignments for the monomer and dimer models, along with their corresponding potential energy distribution (PED) analyses, are provided in Table S2 and S3, respectively.

In the theoretical calculations, anharmonic effects were not considered; consequently, the calculated vibrational wavenumbers were higher than the experimentally observed values. Therefore, the calculated frequencies were corrected using the wavenumber linear scaling (WLS) procedure:

$$\nu_{obs} = (1.0087 - 0.0000163\nu_{cal})\nu_{cal}\ cm^{-1}.$$

The simulated FT-IR spectra of the monomer and dimer APG models were compared with the corresponding experimental spectra, as illustrated in Fig. 4. Table 1 summarizes the stretching vibrational wavenumbers (cm^{-1}) associated with hydrogen bonding, together with the corresponding changes in bond-lengths (Å) for both the monomer and dimer models.

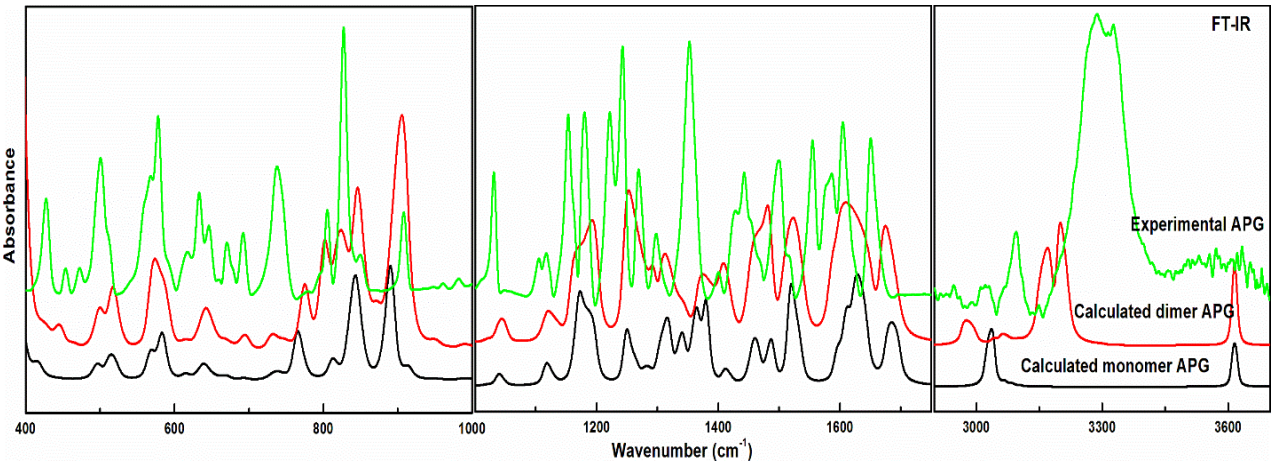


Fig. 4. Observed and calculated (scaled) FT-IR absorbance spectra of APG in the region 400-1000 cm^{-1}, 1001-1750 cm^{-1} and 2900-3700 cm^{-1}.

Table 1. Observed and calculated bond-length in (Å) and stretching wavenumbers in (cm^{-1}) of modes involved in hydrogen bonding in APG.

	C=O group		O-H group		C-H group	
Molecules	**Bond-length**	**Stretching frequency**	**Bond-length**	**Stretching frequency**	**Bond-length**	**Stretching frequency**
Experimental						
APG	1.2819 (C17=O5)	1694 (IR)	0.8412 (O1-H2)	3326 (IR)	0.9499 (C24-H25)	3078 (IR)
	1.3091 (C47=O35)	1586 (IR)	0.8386 (O7-H8)	3208 (IR)		
			0.8394 (O3-H4)	2988 (IR)		
Theoretical						
Monomer	1.2528 (C17=O5)	1686 (IR)	0.9666 (O1-H2)	3618 (IR)	1.0844 (C24H25)	3081 (IR)
			0.9666 (O7-H8)	3614 (IR)		
			0.9998 (O3-H4)	3033 (IR)		
Dimer	1.2550, (C17=O5)	1684 (IR)	0.9665 (O1-H2)	3617 (IR)	1.0853 (C24H25)	3072 (IR)
	1.2691 (C47=O35)	1585 (IR)	0.9897 (O7-H8)	3206 (IR)		
			1.0031 (O3-H4)	2981		

4.2.1 Discussions of modes involved in hydrogen bonding

4.2.1.1 Carbonyl (C=O) group of APG

The (C=O) groups, which act as hydrogen bond acceptors, can readily interact with hydrogen bond donor molecules and are therefore highly sensitive to hydrogen bonding interactions. These groups generally exhibit strong absorption bands in the 1850-1550 cm^{-1} region [41]. In dimer model of APG, the calculated (C=O) stretching vibrations associated with (C17=O5) and (C47=O35) were observed at 1694 and 1586 cm^{-1} in IR spectra corresponding to the calculated peak at 1684 and 1585 cm^{-1}, respectively. The stretching vibrations in monomer model were calculated at 1686 cm^{-1} (given in Table 1) corresponding to the observed peak at 1694 cm^{-1} in IR spectra. Hence, (C17=O5) group is free in monomer and dimer model of APG. The red shifting in stretching wavenumbers of 101 cm^{-1} with increment in calculated bond-length value of 0.0163 Å in dimer, suggest the intermolecular hydrogen bonding (O7-H8···O35) interactions.

4.2.1.2 Hydroxyl (O-H) group of APG

Hydroxyl (O-H) groups can participate actively in hydrogen bonding interactions by functioning as hydrogen bond donors. This (O-H) stretching vibration is highly sensitive to the hydrogen bonding environment and generally appears in the 3200-3700 cm^{-1} region [42]. In monomer/dimer of APG the (O1-H2), (O7-H8) and (O3-H4) group stretching vibrations were calculated at 3618/3617, 3614/3206 and 3033/2981 cm^{-1} corresponding to the observed peak at 3326, 3208 and 2988 cm^{-1}, respectively in IR spectra (as given in Table S2 and S3). The downward shifting in calculated stretching wavenumbers of 408 and 52 cm^{-1} in stretching wavenumbers along with elongation in bond-length value of 0.0231 and 0.1637 Å of (O7-H8) and (O3-H4), respectively from monomer to dimer provide useful evidence for the presence and strength of hydrogen bond interactions in monomer and dimer.

4.2.1.3 (C-H) group of APG

The C-H stretching vibrations are generally observed in the 2800-3100 cm^{-1} spectral region [43]. The frequencies of these vibrations depend on the carbon atom involved and its surrounding chemical environment. In monomer and dimer these (C24-H25) vibrations were calculated at 3081 and 3072 cm^{-1} corresponding to the observed peak at 3078 cm^{-1} in IR spectra region (as given in Table S2 and S3). The (C24-H25) group of APG was directing the formation of intermolecular hydrogen bond interaction (C24-H25···O35).

It was clear from the above discussion that the stretching vibrations and bond-length values of dimer of APG was closer to the experimental values than monomer due to incorporation of nearest possible hydrogen bonding interactions.

4.3 Quantum theory of atoms in molecules (QTAIM) analysis

QTAIM determines the electron density (ED) of every atom in a molecule, which also provides the information regarding the intra- and intermolecular hydrogen bonding to predict the chemical activation of the molecule [44,45]. The ED at bond critical point (BCP) is useful for classification and identification of chemical bonding interactions [45]. The topological parameters (electron density, Laplacian of electron density, kinetic energy density and potential energy density) and geometrical parameters to define the intra- and intermolecular hydrogen bonds in dimer of APG were presented in Table 2.

Table 2. Geometrical parameter (bond-length) and topological parameters for bonds of interacting atoms of intermolecular hydrogen bonding in dimer of APG: electron density (ρ_{BCP}), Laplacian of electron density ($\nabla^2\rho_{BCP}$), electron kinetic energy density (G_{BCP}), electron potential energy density (V_{BCP}), total electron energy density (H_{BCP}) at bond critical point (BCP) and estimated interaction energy (E_{int}).

Hydrogen bonds	**Bond-length (Å)**	**ρ_{BCP} (a.u.)**	**$\nabla^2\rho_{BCP}$ (a.u.)**	**G_{BCP} (a.u.)**	**V_{BCP} (a.u.)**	**H_{BCP} (a.u.)**	**E_{int} (kcal mol^{-1})**
(O3-H4···O5)	1.6544	0.0541	0.1436	0.0040	-0.0439	-0.0399	-13.7738
(O33-H34···O35)	1.7111	0.0466	0.1320	0.0020	-0.0370	-0.0350	-11.6089
(O7-H8···O35)	1.7309	0.0422	0.1191	0.0008	-0.0313	-0.0305	-9.8205
(C48-H49···O7)	2.5515	0.0084	0.0297	-0.0010	-0.0054	-0..0064	- 1.6943
(C24-H25···O35)	2.6824	0.0067	0.0250	-0.0010	-0.0041	-0.0051	-1.2864

The calculated bond-lengths and bond-angles of these corresponding bonds of dimer model of APG were given in Table S4. As per Koch and Popelier criteria, in the dimer of APG, the intermolecular hydrogen bonds has electron density lies in the range (0.002-0.040) a.u. and Laplacian of electron density (0.024-0.139) a.u. [46] In the dimer model, the strength of hydrogen bonds lie in following order; (O3-H4···O5) > (O33-H34···O35) > (O7-H8···O35) > (C48-H49···O7) > (C24-H25···O35), also suggest that these bonds are medium and partially covalent nature, as $H_{BCP} < 0$ and $(\nabla^2\rho_{BCP}) > 0$. The molecular graphs of dimer model of APG are

given in Fig. 5. From Table 2, it is clear that, the intermolecular hydrogen bond (O3-H4···O5) is strongest among all with maximum energy -13.7738 kcal mol^{-1}

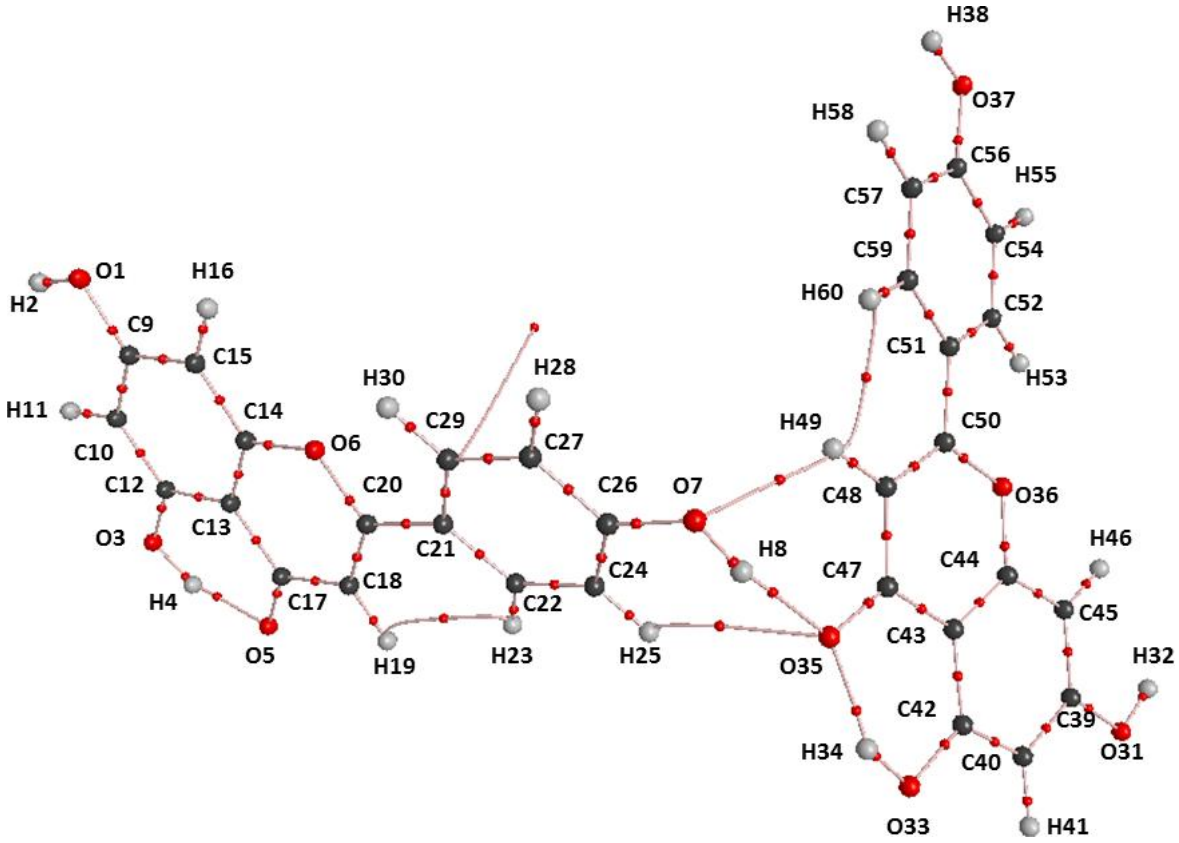


Fig. 5. Molecular graph of dimer of APG: BCPs (small red spheres) and bond paths (pink lines).

4.4 Natural bond orbital (NBO) analysis

NBO analysis is a valuable computational approach for elucidating the electronic structure and bonding characteristics of molecular systems [47]. It provides a localized description of molecular orbitals in terms of Lewis-type bonding and antibonding orbitals, as well as non-Lewis orbitals, including Rydberg and extra-valence orbitals [48]. Furthermore, NBO analysis provides important information regarding intra- and intermolecular interactions in both occupied and unoccupied orbital spaces.

NBO analysis is particularly useful for investigating hyperconjugative interactions and electron density delocalization arising from donor-acceptor interactions between occupied and unoccupied orbitals [49]. Such interactions provide valuable insights into charge-transfer

processes, molecular stability and chemical bonding. The bonding and antibonding orbitals associated with the Lewis structure are generally represented by σ and σ*, respectively [50].

In the present study, NBO analysis was performed for APG dimer by the DFT/B3LYP/6-311G(d,p) level of theory to investigate intramolecular electron delocalization, charge transfer interactions and rehybridization effects. The corresponding NBO parameters are presented in Table S5. As summarized in Table S5, significant intramolecular donor-acceptor interactions were observed within units 1 and 2 of APG dimer, including the interactions LP(2) O3 → π *(C10-C12) and LP(2) O33 → π*(C40-C42) with stabilization energies 42.11 and 40.28 kcal mol^{-1}, respectively were responsible for stabilization of APG dimer. These interactions indicate electron density delocalization from the lone pair orbitals of oxygen atoms to the corresponding antibonding π* orbitals, thereby contributing to the stabilization of the molecular system.

Similarly, the intermolecular charge transfer interactions from unit 1 to unit 2; LP(2) O7 → σ*(C48-H49) and from unit 2 to unit 1; LP(2) O35 → σ*(O7-H8) with $E^{(2)}$ values 0.93 and 13.79 kcal mol^{-1}, responsible for the formation of hydrogen bonds (O7···H49-C48) and (O35···H8-O7), respectively.

4.5 Frontier molecular orbitals (FMOs) and UV-Visible (UV-Vis) spectra

FMOs focus on the highest occupied molecular orbital (HOMO) and lowest unoccupied molecular orbital (LUMO) to define chemical reactivity, stability and electron transport properties in organic molecules [51,52]. A higher HOMO-LUMO energy gap (ΔE) indicates lower reactivity and lower polarizability [53]. One of the concept regarding FMOs are that nucleophiles has donating tendency from their HOMO. In similar way, electrophiles accept into their LUMO.

The HOMO-LUMO plots for the monomer and dimer of APG in the gaseous state are depicted in Figs. S2 and 6, respectively. The ΔE values of monomer and dimer were noticed to be 4.8127 and 3.2890 eV, respectively. Since, the dimer model has smaller energy gap than monomer, hence requires less energy for electron excitation, so decreases its kinetic stability and increases its chemical reactivity and polarizability.

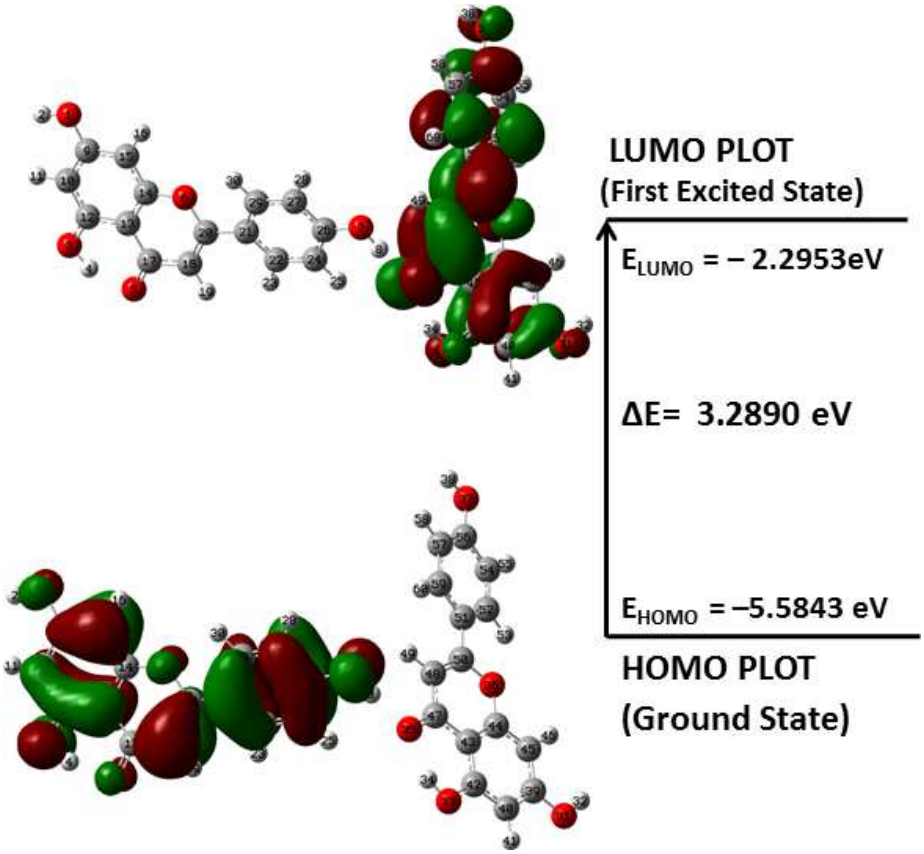


Fig. 6. HOMO-LUMO plot of dimer of APG with orbital involved in electronic transitions.

For the understanding of electronic transitions of the title molecular system, UV-Visible spectroscopic analysis has been performed using IEF-PCM (Integral Equation Formalism Polarizable Continuum) model with 6-311G(d,p) basis set [54,55]. The absorption bands were recorded in methanol solvent as well as calculated in gaseous phase using TD-DFT method with B3LYP functional [56,57]. Experimentally observed spectra of APG showed three absorption bands in the region 200-400 nm and shown in Fig. 7. To gain insight into the nature of the electronic transitions of the APG molecule, the observed absorption peaks, calculated absorption maxima (λ_{max}), oscillator strengths (f), and the corresponding electronic transition assignments were systematically analyzed and the results are presented in Table 3.

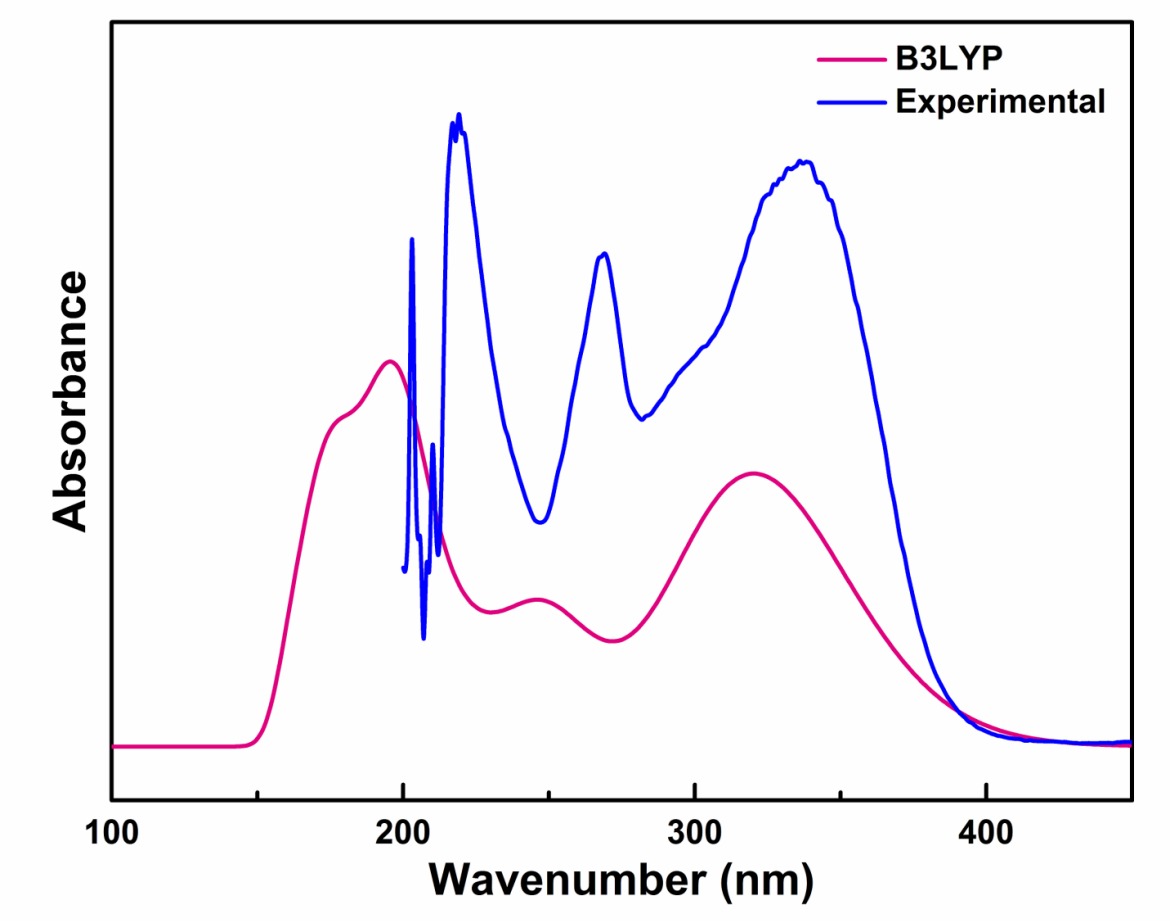


Fig. 7. Experimental and calculated UV-Visible spectrum of APG in methanol solvent.

Table 3. Electronic transitions, absorption peaks λ_{max} (nm), oscillator strength (f), excitation energy (eV), and assignments of the transitions of APG.

Excited state	Experimental methanol	Functional	Calculated (Methanol)				
	λmax (nm)		λmax (nm)	E(eV)	Oscillator strength (f)	Excitation transition	Assignment
1	337	B3LYP	339	3.6526	0.3053	H→L	π→π*
2	268	B3LYP	266	4.6607	0.0024	H-4→L	σ→π*
3	218	B3LYP	216	5.7478	0.0776	H→L+3	π→π*

HOMO (highest occupied molecular orbital) and LUMO (Lower unoccupied molecular orbital) are the prominent orbitals which take part in chemical reactions and are responsible for charge transfer properties. The first absorption band was calculated (B3LYP) at 339 nm with oscillator strength 0.3053 corresponding to the observed peak at 337 nm. This band corresponds to H→L

transition (π→π*). Second absorption band was recorded at 268 nm which is attributed towards 266 nm in B3LYP. The transition originates from H-4→L (B3LYP) with π→π* transition. Third transition mainly corresponds to π→π* with an experimentally recorded absorption band at 218 nm and calculated band at 216 nm in B3LYP the functional (shown in Fig. 8).

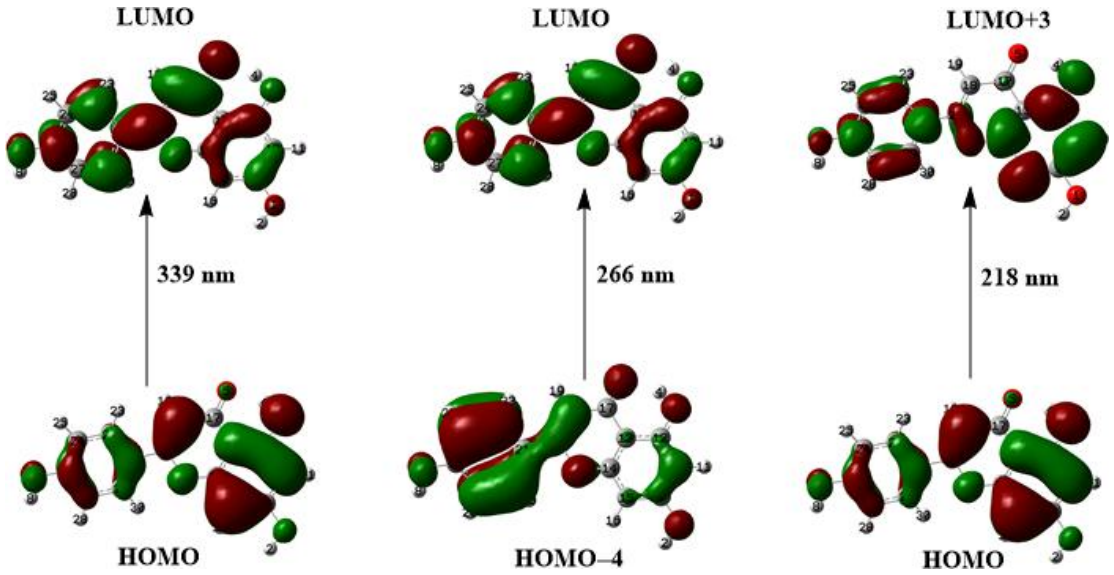


Fig. 8 HOMO-LUMO plots for the selected transitions of APG

The molecular orbital analysis of APG revealed that its electronic structure is predominantly composed of p orbitals. Consequently, the observed electronic transitions are mainly attributed to π→ π* excitation, as summarized in Table 3. UV-Visible spectral analysis was examined using B3LYP functional. This study suggests that results of B3LYP functional were found to be much better w.r.t experimental findings.

4.6 Chemical reactivity descriptors

4.6.1 Global reactivity descriptor parameters

The molecular chemical behavior is defined by using global reactivity descriptors, such as electronegativity (χ), chemical potential (μ), hardness (η), electrophilicity index (ω) and softness (S) calculated by means of E_{HOMO}, E_{LUMO} [58-60] for monomer and dimer model of APG are listed in Table 4.

Table 4 Calculated E_{HOMO}, E_{LUMO}, energy gap (E_L-E_H), ionization potential (I), electron affinity (A), electronegativity (χ), global hardness (η), global softness (S) chemical potential (μ) and global electrophilicity index (ω) at 298.15 K for monomer and dimer models of APG.

Molecules	E_{HOMO} (eV)	E_{LUMO} (eV)	$\Delta E=(E_L-E_H)$ (eV)	I (eV)	A (eV)	χ (eV)	H (eV)	S (eV^{-1})	M (eV)	ω (eV)
Monomer of APG	-5.9427	-1.7600	4.8127	5.9427	1.7600	3.8513	2.0913	0.2391	-3.8513	3.5462
Dimer of APG	-5.5843	-2.2953	3.2890	5.5843	2.2953	3.9398	1.6445	0.3040	-3.9398	4.7194

The parameters ionization potential (I) of APG dimer (5.5843 eV) < monomer (5.9427 eV), showing that an electron can remove easily from the dimer in comparison to that of monomer. The lower energy gap (3.2890 eV) of dimer of APG indicates that dimer is more reactive (less stable) than monomer. The electron affinity of dimer (2.2953 eV) > monomer (1.7600 eV), hence, dimer has better electron accepting properties. The global hardness (η) of dimer (1.6445 eV) < monomer (2.0913 eV), which means dimer is softer than that of monomer.

4.6.2 Local reactivity descriptors

Fukui functions $f(r)$ can usually predict the most reactive nucleophilic and electrophilic sites of the molecules [61,62]. The larger positive values of $f_k(r)$ indicates nucleophilic attack, whereas the larger negative values of $f_k(r)$ is subjected to electrophilic attack. These local reactivity descriptors for monomer and dimer of APG were given in Tables S6 and S7, respectively.

From Table S6, the maximum values of $(f_k^+, s_k^+, \omega_k^+)$ in monomer model of APG were (0.0800, 0.0150, 0.1630) for O3, reveals that it is suitable to nucleophilic attack. In similar way, the maximum value of $(f_k^-, s_k^-, \omega_k^-)$ is (0.0866, 0.0162, 0.1765) for O5 making it suitable for electrophilic attack. Similarly, in dimer model of APG, the maximum values of $(f_k^+, s_k^+, \omega_k^+)$ were found to be (0.0586, 0.0110, 0.1194) for C18 and $(f_k^-, s_k^-, \omega_k^-)$ were (0.0638, 0.0119, 0.1300) for C50, makes them suitable for nucleophilic and electrophilic attack, respectively (as given in Table S7).

4.7 Molecular electrostatic potential surface (MESP)

In computational chemistry and bioinformatics, MESP plays a pivotal role to predict the drug design and illustrating molecular interactions [63,64]. MESP map represents the electrostatic interaction energy which is essential to visualize 3D charge distribution. This map is useful to probe the non-covalent interactions (like hydrogen bonding and halogen bonding), polarity and molecular reactivity [64]. It reveals nucleophilic and electrophilic regions on molecular map to define better understating of chemical reactions. The MESP isosurfaces of monomer and dimer of APG are depicted in Figs. S3 and 9, respectively.

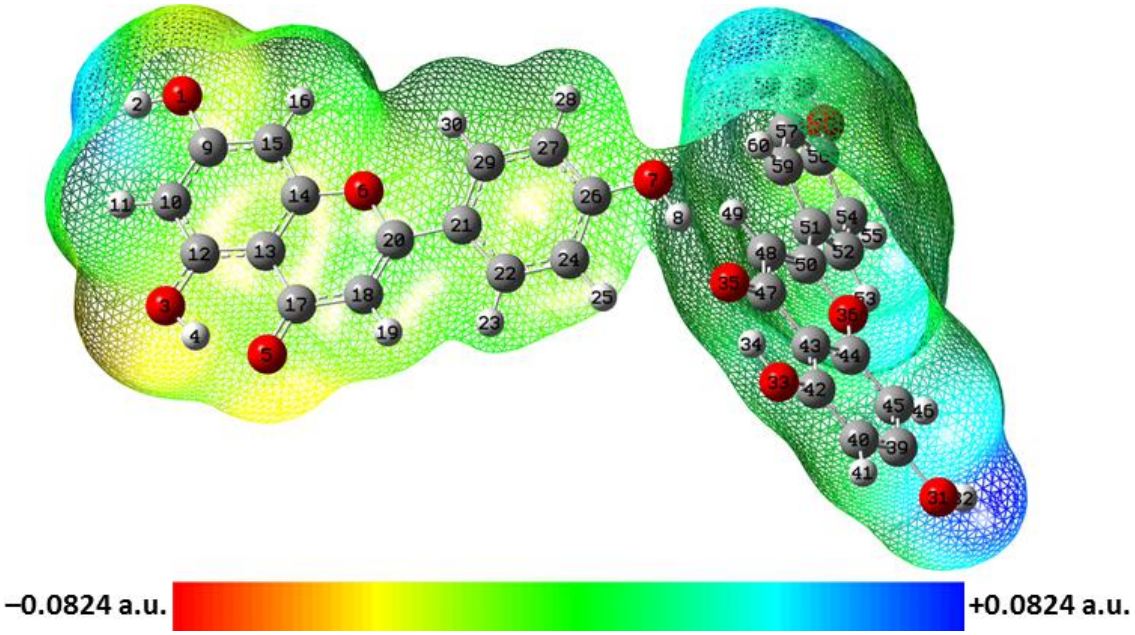


Fig. 9. Molecular electrostatic potential (MESP) formed by mapping of total density over electrostatic potential in the gas phase for dimer of APG.

The MESP isosurface of monomer model of APG shows that red region is over carbonyl (C17=O5) and blue region is distributed over hydroxyl (O7-H8) and hence suitable for electrophilic and nucleophilic attack, respectively (shown in Fig. S3). Similarly in dimer model of APG, the electrophilic reactivity of (C17=O5) and nucleophilic reactivity of (O7-H8) neutralizes due to hydrogen bond interactions (O7-H8…O35) and (O3-H4…O5), respectively (as shown in Fig. 9).

4.8 Molar refractivity (MR)

MR is an important physicochemical descriptor in drug designing used to identifies total polarizability per mole of a substance, molar volume and bulk state [65,66]. Lipinski's rule of

five (RO5) [66] is helpful to distinguish between drug like and non-drug like behavior of the molecules. RO5 states that (a) Molecular mass < 500 Dalton, (b) High lipophilicity (LogP < 5) (c) Less than 5 hydrogen bond donors and (d) Less than 10 hydrogen bond acceptor.

The molecules having; (a) molar refractivity (MR) values within 40-130 e.s.u., (b) the number of atoms lie between 20-70, (c) the molecular weight of 180-500 g mol^{-1} were also like to follow permeability and absorption of drug molecules.

The MR values of monomer and dimer of APG were calculated to be 41.13 and 79.11 e.s.u., respectively. The molecular weights of monomer of APG were 270.24 g mol^{-1}. Additionally, the numbers of atoms in monomer and dimer of APG were 30 and 60, respectively. Hence, as per above criteria, APG follows these rules and hence possess drug-like property.

4.9 Molecular docking of apigenin

Molecular docking was performed to understand the process of ligand (drug) and receptor (proteins) binding interaction, identification of binding atomic sites of that reveals the binding affinity and is an important part of designing of drugs [67]. This method has become a crucial component of in silico drug development [68]. Previous studies reveal that APG as a potential treatment for neurological disorders, cardiovascular disease, antitumor treatment, leukemia, lung and prostate cancer, etc. [69,70] Molecular docking is a structure-function relation of APG and has been reported with many receptors [71]. SwissDock prediction was used to select the different targets to understand the docking between APG and recepators [72].

In this work, in order to predict the biological properties of APG, the molecular docking with death-associated protein kinase 1 (DAPK1) in complex with 1-anilinonaphthalene-8-sulfonic acid (ANS) (PDB code; 5AUT) [23], severe acute respiratory syndrome coronavirus 2 (SARS-CoV-2, PDB code: 7ZH5) [24] and acetylcholinesterase (PDB code: 1EEA) [25]. These structures were retrieved from RCSB protein data bank. The docking mechanism revealed the binding interactions of these transferase, viral protein, oxidoreductase and hydrolase, respectively with ligand (apigenin). The active binding sites of these aforesaid receptors were described to include residues on the grid size of 60 Å × 60 Å ×60 Å. The receptor was prepared by removing water, cofactors and Lamarckian Genetic Algorithm (LGA) present in Autodock, which was further employed for docking. Out of all possible docked conformations, which bind

better within the reactive sites were chosen to be considered, further detailed interactions were visualized into Discovery Studio Visualizer 4.5 software, pictured in Fig. 10, respectively. The calculated values of binding energy (kcal/mol), inhibition constant Ki (μm), intermolecular energy (kcal/mol) and hydrogen bonds with binding sites (Å) were obtained from output clusters of Autodock 4.2 have been reported in Table 5.

Table 5 Binding energies, inhibition constants and interaction energies of apigenin (APG) against protein targets death associated protein kinase 1 (human) complex with 1-anilinonaphthalene-8-sulfonic acid (ANS),(PDB code: 5AUT) SARS CoV Spike Protein (pdb CODE: 7ZHF) and acetylcholinesterase (AChE) (PDB code:1EEA) using Autodock 4.2.

Targets	Binding energy (kcal/mol)	Inhibition constant Ki (μm)	Intermolecular energy (kcal/mol)	Hydrogen bonds with binding sites (Å)
5AUT	-5.37	116.42	-6.86	2.29 (H8):GLU100 2.47 (H4): ASP139 1.94(O5): ASN144
7ZHF	-6.57	15.19	-8.07	2.04 (H2): GLN936 2.28 (H19):GLN744 1.95 (H8): SER985
1EEA	-6.35	22.31	-6.35	1.96 (H2): HIS 440 1.96 (H4): GLU199 2.01 (O3): TYR130 1.83 (H8):TYR70

From Table 5, it is clear that among all targets, APG forms stronger hydrogen bonds with GLN744, SER985, HIS440 of 7ZHF with distances 2.28, 1.95 and 1.96 Å, respectively (depicted in Fig. 10 (b) also possesses lowest binding energy -6.57 kcal/mol. Additionally, the lowest value of Ki (15.19 μm) for 7ZHF suggests it as suitable bioreceptors, as low amount of medication will be required for the inhibition of the enzyme activity.[13] Hence, it is clear that the severe acute respiratory syndrome coronavirus 2 property of APG is the most significant among all other targets.

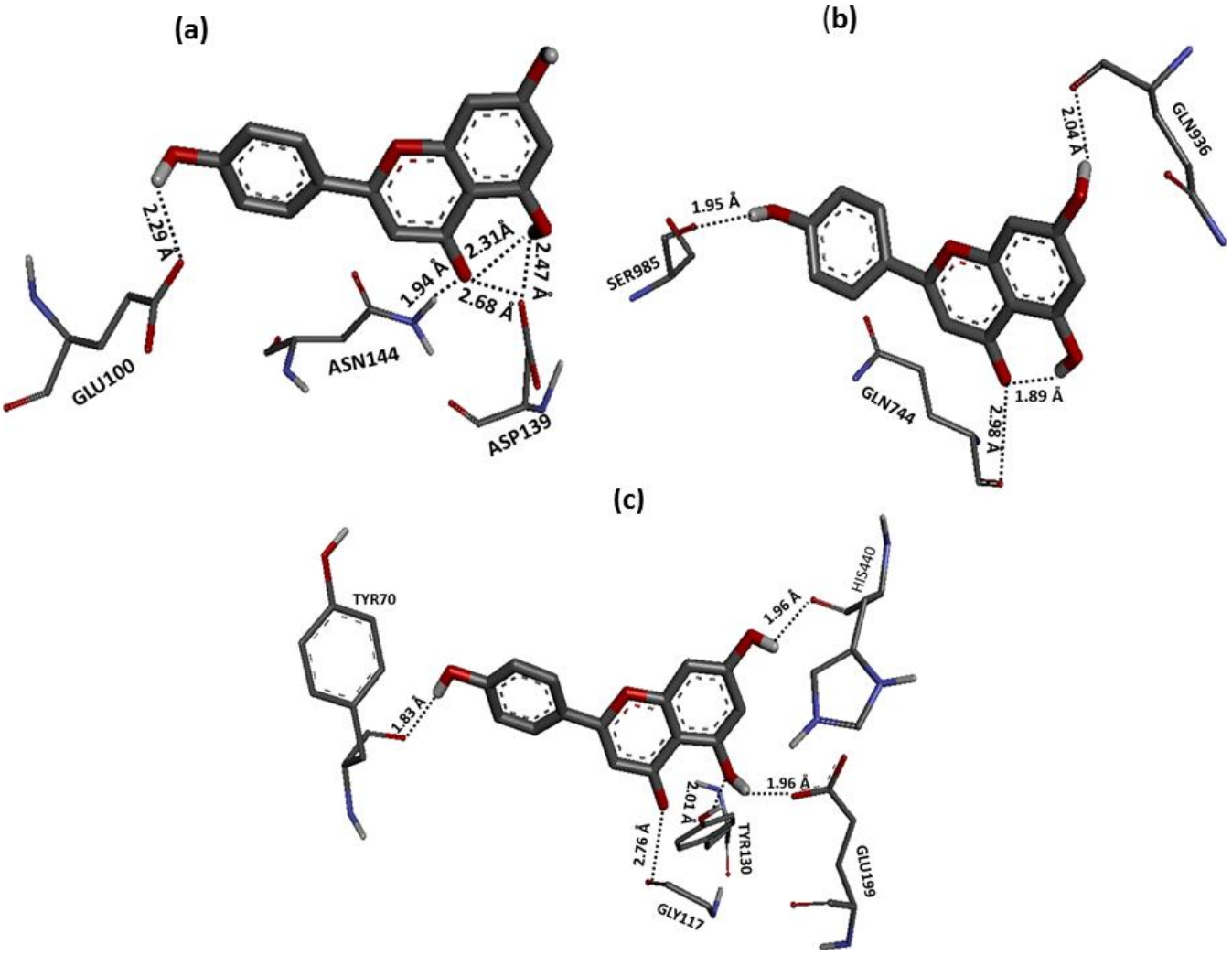


Fig. 10 (a) Docking picture of APG with 5AUT, (b) docking picture of APG with 7ZHF, (c) docking picture of APG with 1EEA.

5. Conclusions

In the present study, structural, vibrational, hydrogen bonding interactions and reactivity analysis of APG were done by quantum chemical calculations and FT-IR spectroscopy technique. The monomer and dimer models of APG were explored by DFT/B3LYP/6-311G(d,p) methodology. The structural analysis revealed that intermolecular hydrogen bonding interactions (O3-H4···O5), (O33-H34···O35), (O7-H8···O35), (C48-H49···O7) and (C24-H25···O35) were present in dimer model. The bond-lengths and bond-angles were in excellent correlation with theoretical values of dimer in comparison to monomer model of APG. Additionally, the red shifting and stretching

wavenumbers of (C=O) and (O-H) groups revealed that these groups are involved in intermolecular hydrogen bonds and hence formation of dimer model. The QTAIM analysis showed that all the aforesaid hydrogen bonds were medium and partially covalent in nature, as $H_{BCP} < 0$ and $(\nabla^2\rho_{BCP}) > 0$. Additionally, (O3-H4···O5) is strongest intermolecular hydrogen bond among all with maximum energy -13.7738 kcal mol^{-1}. The NBO analysis the intermolecular charge transfer interactions from unit 1 to unit 2; LP(2) O7 → σ*(C48-H49) and from unit 2 to unit 1; LP(2) O35 → σ*(O7-H8) were responsible for stabilization of dimer model of APG. The dimer model is more reactive and less stable than monomer, due to low HOMO-LUMO energy gap. The lowering in HOMO-LUMO energy gap proves the charge transfer in the dimer model of APG. MESP map showed that nucleophilic and electrophilic reactive sites were neutralized in dimer model, due to the presence of intermolecular hydrogen bondings. Moreover, APG followed all rules of Lipinski's rule of five, hence it can be used as drug likeness. The molecular docking studies showed that APG has relatively more binding energy with the target 7ZHF. Hence, this work may provide useful insights into the therapeutic potential of APG as a bioactive molecule.

Acknowledgments

The authors gratefully acknowledge the Department of Science and Technology (DST), New Delhi, India, for financial support provided to AS under the Women Scientist Scheme (WOS A) for Research in Basic/Applied Sciences, award no. DST/WOS-A/CS-110/2021. PV and AS sincerely acknowledge the Central Facility for Computational Research (CFCR), University of Lucknow, Lucknow, India, for providing computational resources. The authors also acknowledge the PAIR Network of SAKSHAM funded by Anusandhan National Research Foundation), India, through grant ANRFPAIR/2025/000018/PAIR, administered and mentored by IIT Indore.

Data availability

All data generated or analysed during this study are included in this published article [and its supplementary information files].

Ethics declarations

Ethics approval and consent to participate

Not applicable.

Consent for publication

Not applicable

Competing interests

The authors declare no competing interests

References

[1] Naponelli V, Rocchetti MT, Mangieri D. Apigenin: molecular mechanisms and therapeutic potential against cancer spreading. Int J Mol Sci. 2024;25(10):5569.

[2] Siddiquee R, Mahmood T, Ansari VA, Ahsan F, Bano S, Ahmad S. Apigenin unveiled: an encyclopedic review of its preclinical and clinical insights. Discover Plants. 2025;2(1):11.

[3] Kashyap D, Sharma A, Tuli HS, Sak K, Garg VK, Buttar HS, Sethi G. Apigenin: a natural bioactive flavone-type molecule with promising therapeutic function. J Funct Foods. 2018;48:457-471.

[4] Rahul F, Naz F, Jyoti S, Siddique YH. Health functionality of apigenin: a review. Int J Food Prop. 2017;20(6):1197-1238.

[5] Singh A, Singh J, Parween G, Khator R, Monga V. A comprehensive review of apigenin, a dietary flavonoid: biological sources, nutraceutical prospects, chemistry, pharmacological insights and health benefits. Crit Rev Food Sci Nutr. 2025;65(23):4529-4565.

[6] Waheed A, Zameer S, Ashrafi K, Ali A, Sultana N, Aqil M, Iqbal Z. Insights into pharmacological potential of apigenin through various pathways on a nanoplatform in multitude of diseases. Curr Pharm Des. 2023;29(17):1326-1340.

[7] Tang D, Chen K, Huang L, Li J. Pharmacokinetic properties and drug interactions of apigenin, a natural flavone. Expert Opin Drug Metab Toxicol. 2017;13(3):323-330.

[8] Salehi B, Venditti A, Sharifi-Rad M, Kregiel D, Sharifi-Rad J, Durazzo A, Martins N. The therapeutic potential of apigenin. Int J Mol Sci. 2019;20(6):1305.

[9] Li Z, Zhou J, Ji L, Liang Y, Xie S. Recent advances in the pharmacological actions of apigenin, its complexes, and its derivatives. Food Rev Int. 2023;39(9):6568-6601

[10] Makadia J, Seaton CC, Li M. Apigenin cocrystals: from computational prescreening to physicochemical property characterization. Cryst Growth Des. 2023;23(5):3480-3495.
[11] Jiang X, Huang H. The therapeutic potential of apigenin against atherosclerosis. Heliyon. 2025;11(1):e41272.
[12] Lin S, Yincang W, Jiazhe D, Xilin X, Zhang X. Pharmacology and mechanisms of apigenin in preventing osteoporosis. Front Pharmacol. 2024;15:1486646.
[13] Mariappan G, Sundaraganesan N, Manoharan S. The spectroscopic properties of anticancer drug apigenin investigated by using DFT calculations, FT-IR, FT-Raman and NMR analysis. Spectrochim Acta A Mol Biomol Spectrosc. 2012;95:86-99.
[14] Kohn W, Becke AD, Parr RG. Density functional theory of electronic structure. J Phys Chem. 1996;100(31):12974-12980.
[15] Chaachouay N, Zidane L. Plant-derived natural products: a source for drug discovery and development. Drugs Drug Candidates. 2024;3(1):184-207.
[16] Newman DJ, Cragg GM, Snader KM. The influence of natural products upon drug discovery. Nat Prod Rep. 2000;17(3):215-234.
[17] Mazumdar P, Kashyap A, Choudhury D. Investigation of hydrogen bonding in small nucleobases using DFT, AIM, NCI and NBO technique. Comput Theor Chem. 2023;1226:114188.
[18] Miar M, Shiroudi A, Pourshamsian K, Oliaey AR, Hatamjafari F. Theoretical investigations on the HOMO-LUMO gap and global reactivity descriptor studies, natural bond orbital, and nucleus-independent chemical shifts analyses of 3-phenylbenzo[d]thiazole-2(3H)-imine and its para-substituted derivatives: solvent and substituent effects. J Chem Res. 2021;45(1-2):147-158.
[19] Chermette H. Chemical reactivity indexes in density functional theory. J Comput Chem. 1999;20(1):129-154.
[20] Pal R, Chattaraj PK. Electrophilicity index revisited. J Comput Chem. 2023;44(3):278-297.
[21] Meng XY, Zhang HX, Mezei M, Cui M. Molecular docking: a powerful approach for structure-based drug discovery. Curr Comput-Aided Drug Des. 2011;7(2):146-157.
[22] Raval K, Ganatra T. Basics, types and applications of molecular docking: a review. IP Int J Compr Adv Pharmacol. 2022;7(1):12-16.
[23] Farag AK, Roh EJ. Death-associated protein kinase (DAPK) family modulators: current and future therapeutic outcomes. Med Res Rev. 2019;39(1):349-385.

[24] Shitrit A, Zaidman D, Kalid O, Bloch I, Doron D, Yarnizky T, Kobiler O. Conserved interactions required for inhibition of the main protease of severe acute respiratory syndrome coronavirus 2 (SARS-CoV-2). Sci Rep. 2020;10(1):20808.
[25] Fernandes TB, Cunha MR, Sakata RP, Candido TM, Baby AR, Tavares MT, Parise-Filho R. Synthesis, molecular modeling, and evaluation of novel sulfonylhydrazones as acetylcholinesterase inhibitors for Alzheimer's disease. Arch Pharm. 2017;350(11):1700163.
[26] Lee C, Yang W, Parr RG. Development of the Colle-Salvetti correlation-energy formula into a functional of the electron density. Phys Rev B. 1988;37(2):785.
[27] Parr RG. Density functional theory of atoms and molecules. In: Horizons of Quantum Chemistry: Proceedings of the Third International Congress of Quantum Chemistry, Kyoto, Japan, October 29-November 3, 1979. Dordrecht: Springer Netherlands; 1989. pp. 5-15.
[28] Del Bene JE, Person WB, Szczepaniak K. Properties of hydrogen-bonded complexes obtained from the B3LYP functional with 6-31G(d,p) and 6-31+G(d,p) basis sets: comparison with MP2/6-31+G(d,p) results and experimental data. J Phys Chem. 1995;99(27):10705-10707.
[29] Frisch MJ, Trucks GW, Schlegel HB, Scuseria GE, Robb MA, Cheeseman JR, et al. Gaussian 09, revision [version not specified]. Wallingford: Gaussian Inc.; 2009.
[30] Frisch A, Nielson AB, Holder AJ. GaussView user manual. Pittsburgh: Gaussian Inc.; 2000.
[31] Martin JML, Van Alsenoy C. GAR2PED. Antwerp: University of Antwerp; 1995.
[32] Yoshida H, Takeda K, Okamura J, Ehara A, Matsuura H. A new approach to vibrational analysis of large molecules by density functional theory: wavenumber-linear scaling method. J Phys Chem A. 2002;106(14):3580-3586.
[33] Bader RFW, Cheeseman JR. AIMPAC: a suite of programs for the AIM theory. Hamilton: McMaster University; 2000.
[34] Espinosa E, Molins E, Lecomte C. Hydrogen bond strengths revealed by topological analyses of experimentally observed electron densities. Chem Phys Lett. 1998;285(3-4):170-173.
[35] Sujatha HS, Lavanya M. An insight to HOMO-LUMO aspects in corrosion applications. Can Metall Q. 2023;62(4):761-772.
[36] Bhatia M. An overview of conceptual-DFT based insights into global chemical reactivity of volatile sulfur compounds (VSCs). Comput Toxicol. 2024;29:100295.
[37] Hansch C, Verma RP. Understanding tubulin/microtubule-taxane interactions: a quantitative structure-activity relationship study. Mol Pharm. 2008;5(1):151-161.

[38] Morris GM, Huey R, Lindstrom W, Sanner MF, Belew RK, Goodsell DS, Olson AJ. AutoDock4 and AutoDockTools4: automated docking with selective receptor flexibility. J Comput Chem. 2009;30(16):2785-2791.
[39] Accelrys Inc. Discovery Studio 4.5 guide. San Diego: Accelrys Inc.; 2009.
[40] Guan H, Sun H, Zhao X. Application of density functional theory to molecular engineering of pharmaceutical formulations. Int J Mol Sci. 2025;26(7):3262.
[41] Lorenz-Fonfria VA. Infrared difference spectroscopy of proteins: from bands to bonds. Chem Rev. 2020;120(7):3466-3576.
[42] Bandyopadhyay A, Saha G, Mondal JA. Vibrational coupling and hydrogen-bond structure of water in the extended hydration shell of metal ions. J Phys Chem B. 2023;127(32):7174-7180.
[43] Yu Y, Lin K, Zhou X, Wang H, Liu S, Ma X. New C-H stretching vibrational spectral features in the Raman spectra of gaseous and liquid ethanol. J Phys Chem C. 2007;111(25):8971-8978.
[44] Saidj M, Djafri A, Rahmani R, Belkafouf NEH, Boukabcha N, Djafri A, Chouaih A. Molecular structure, experimental and theoretical vibrational spectroscopy, (HOMO-LUMO, NBO) investigation, (RDG, AIM) analysis, (MEP, NLO) study and molecular docking of ethyl-2-{[4-ethyl-5-(quinolin-8-yloxymethyl)-4H-1,2,4-triazol-3-yl]sulfanyl} acetate. Polycycl Aromat Compd. 2023;43(3):2152-2176.
[45] Afonin AV, Rusinska-Roszak D. Quantification of hydrogen bond energy based on equations using spectroscopic, structural, QTAIM-based, and NBO-based descriptors calibrated by the molecular tailoring approach. J Mol Model. 2024;30(1):18.
[46] Koch U, Popelier PL. Characterization of C-H-O hydrogen bonds on the basis of the charge density. J Phys Chem. 1995;99(24):9747-9754.
[47] Agwupuye JA, Louis H, Unimuke TO, David P, Ubana EI, Moshood YL. Electronic structure investigation of the stability, reactivity, NBO analysis, thermodynamics, and the nature of the interactions in methyl-substituted imidazolium-based ionic liquids. J Mol Liq. 2021;337:116458.
[48] Halim SA, El-Meligy AB, El-Nahas AM, El-Demerdash SH. DFT study and natural bond orbital (NBO) population analysis of 2-(2-hydroxyphenyl)-1-azaazulene tautomers and their mercapto analogues. Sci Rep. 2024;14(1):219.

[49] Susheel, Alsubaie AS, Ahmed M, Malhotra SS, Asha, Gupta MK, Ansari A. DFT and TDDFT studies on pi-conjugated ligands for copper sensing: analyzing electronic structures and optical performance. J Mol Model. 2025;31(11):306.
[50] Santos RA, Santos CV Jr, Aguiar EC, Carneiro Neto AN, Moura RT Jr. Orbital interactions in hydrogen bonds: a perspective from the chemical bond overlap model. J Comput Chem. 2025;46(19):e70166.
[51] Shahab S, Sheikhi M, Filippovich L, Dikusar E, Darroudi M, Kaviani S, Drachilovskaya M. Optimization, spectroscopic (excited states, UV/Vis, polarization) studies, FMO, ELF, LOL, QTAIM, NBO analysis and electronic properties of two new azomethine derivatives: theoretical and experimental investigations. Russ J Phys Chem A. 2020;94(9):1848-1865.
[52] Akram SJ, Hadia NMA, Shawky AM, Iqbal J, Khan MI, Alatawi NS, Khera RA. Designing thiophene[3,2-b]pyrrole ring-based NFAs for high-performance electron transport materials: a DFT study. ACS Omega. 2023;8(12):11118.
[53] Miar M, Shiroudi A, Pourshamsian K, Oliaey AR, Hatamjafari F. Theoretical investigations on the HOMO-LUMO gap and global reactivity descriptor studies, natural bond orbital, and nucleus-independent chemical shifts analyses of 3-phenylbenzo[d]thiazole-2(3H)-imine and its para-substituted derivatives: solvent and substituent effects. J Chem Res. 2021;45(1-2):147-158.
[54] Bourass M, Benjelloun AT, Benzakour M, Mcharfi M, Hamidi M, Bouzzine SM, Bouachrine M. DFT and TD-DFT calculation of new thienopyrazine-based small molecules for organic solar cells. Chem Cent J. 2016;10(1):67.
[55] Etabti H, Fitri A, Benjelloun AT, Hachi M, Benzakour M, Mcharfi M. Benzocarbazole-based D-Di-pi-A dyes for DSSCs: DFT/TD-DFT study of influence of auxiliary donors on the performance of free dye and dye-TiO2 interface. Res Chem Intermed. 2021;47(10):4257-4280.
[56] El-Shishtawy RM, Elroby SA, Asiri AM, Mullen K. Optical absorption spectra and electronic properties of symmetric and asymmetric squaraine dyes for use in DSSC solar cells: DFT and TD-DFT studies. Int J Mol Sci. 2016;17(4):487.
[57] Sherefedin U, Belay A, Gudishe K, Kebede A, Kumela AG, Wakjira TL, Gelanu D. Investigating the effects of solvent polarity and temperature on the molecular, photophysical, and thermodynamic properties of sinapic acid using DFT and TDDFT. RSC Adv. 2024;14(32):23364-23377.
[58] Pal R, Chattaraj PK. Electrophilicity index revisited. J Comput Chem. 2023;44(3):278-297.

[59] Radhi AH, Du EA, Khazaal FA, Abbas ZM, Aljelawi OH, Hamadan SD, Kadhim MM. HOMO-LUMO energies and geometrical structures effect on corrosion inhibition for organic compounds predicted by DFT and PM3 methods. NeuroQuantology. 2020;18(1):37-45.
[60] Choudhary V, Bhatt A, Dash D, Sharma N. DFT calculations on molecular structures, HOMO-LUMO study, reactivity descriptors and spectral analyses of newly synthesized diorganotin(IV) 2-chloridophenylacetohydroxamate complexes. J Comput Chem. 2019;40(27):2354-2363.
[61] Zamora PP, Bieger K, Cuchillo A, Tello A, Muena JP. Theoretical determination of a reaction intermediate: Fukui function analysis, dual reactivity descriptor and activation energy. J Mol Struct. 2021;1227:129369.
[62] Roy DR, Parthasarathi R, Maiti B, Subramanian V, Chattaraj PK. Electrophilicity as a possible descriptor for toxicity prediction. Bioorg Med Chem. 2005;13(10):3405-3412.
[63] Kumar B, Devi J, Dubey A, Kumar M. Biological and computational studies of hydrazone-based transition metal(II) complexes. Chem Biodivers. 2024;21(11):e202401116.
[64] Bhardwaj A, Dubey A, Tufail A, Tufail N, Kumar M, Garg S. Unveiling the biomedical potential of thiophene-derived Schiff base complexes: a comprehensive study of synthesis, spectral characterization, antimicrobial efficacy, antioxidant activity, and computational insights. Appl Organomet Chem. 2024;38(5):e7398.
[65] Raevsky OA. Physicochemical descriptors in property-based drug design. Mini Rev Med Chem. 2004;4(10):1041-1052.
[66] Le J. The calculation of physicochemical descriptors and their application in predicting properties of drugs and other compounds [dissertation]. London: University College London, University of London; 2001.
[67] Naqvi AA, Mohammad T, Hasan GM, Hassan MI. Advancements in docking and molecular dynamics simulations towards ligand-receptor interactions and structure-function relationships. Curr Top Med Chem. 2018;18(20):1755-1768.
[68] Muhammed MT, Aki-Yalcin E. Molecular docking: principles, advances, and its applications in drug discovery. Lett Drug Des Discov. 2024;21(3):480-495.
[69] Pandita G, Mittal D, Kashyap P, Lai WF, Kumar N, Mehra R, Ashraf SA. Apigenin and its derivatives in breast cancer prevention and therapy: a review on bioavailability and recent development. Phytomed Plus. 2025;5(4):100870.

[70] Kumar G, Jain P, Virmani T, Sharma A, Akhtar MS, Aldosari SA, Fonte P. Enhancing therapy with nano-based delivery systems: exploring the bioactive properties and effects of apigenin. Ther Deliv. 2024;15(9):717-735.
[71] Peanlikhit T, Aryal U, Welsh JS, Shroyer KR, Rithidech KN. Evaluation of the inhibitory potential of apigenin and related flavonoids on various proteins associated with human diseases using AutoDock. Int J Mol Sci. 2025;26(6):2548.
[72] Kumar A, Reza MI, Banerjee A, Ambhore NS, Balraj P, Layek B, Sathish V. 2-Hydroxyestradiol regulates extracellular matrix deposition through estrogen receptor beta activation in airway smooth muscle cells. Mol Cell Endocrinol. 2026;615:112753.

Supplementary Files

This is a list of supplementary files associated with this preprint. Click to download.

- RevisedSupplementaryMaterial.docx
- SupplementaryMaterial.docx